

An Assembly Automation Approach to Alignment of Noncircular Projections in Electron Microscopy

Wooram Park, *Member, IEEE*, and Gregory S. Chirikjian, *Fellow, IEEE*

Abstract—In single-particle electron microscopy (EM), multiple micrographs of identical macromolecular structures or complexes are taken from various viewing angles to obtain a 3D reconstruction. A high-quality EM reconstruction typically requires several thousand to several million images. Therefore, an automated pipeline for performing computations on many images becomes indispensable. In this paper, we propose a modified cross-correlation method to align a large number of images from the same class in single-particle electron microscopy of highly nonspherical structures, and show how this method fits into a larger automated pipeline for the discovery of 3D structures. Our modification uses a probability density in full planar position and orientation, akin to the pose densities used in Simultaneous Localization and Mapping (SLAM) and Assembly Automation. Using this alignment and a subsequent averaging process, high signal-to-noise ratio (SNR) images representing each class of viewing angles are obtained for reconstruction algorithms. In the proposed method, first we coarsely align projection images, and then realign the resulting images using the cross correlation (CC) method. The coarse alignment is obtained by matching the centers of mass and the principal axes of the images. The distribution of misalignment in this coarse alignment is estimated using the statistical properties of the additive background noise. As a consequence, the search space for realignment in the CC method is reduced. Additionally, in order to overcome the false peak problems in the CC, we use artificially blurred images for the early stage of the iteration and segment the intermediate result from every iteration step. The proposed approach is demonstrated on synthetic noisy images of GroEL/ES.

Note to Practitioners—This paper concerns the automated alignment of the large number of noisy images that must be handled when class averaging is applied in single-particle electron microscopy. The new proposed method consists of prealignment, iterative alignment using the CC, artificial image blurring and image segmentation. The prealignment is obtained by matching the center of mass and the principal axis of the images. This results in a SLAM-like distribution of pose with quantifiable covariance, on which computations can be performed. Next the prealigned images are aligned more accurately through the iterative CC method with image blurring and segmentation. The most notable improvement is the prealignment step. Although this

Manuscript received May 29, 2013; revised September 21, 2013; accepted December 03, 2013. Date of publication January 09, 2014; date of current version June 30, 2014. This paper was recommended for publication by Associate Editor H. Tanner and Editor A. Bicchi upon evaluation of the reviewers' comments. This work was supported by the National Science Foundation under Grant IIS-1162095.

W. Park is with the Department of Mechanical Engineering, University of Texas at Dallas, Richardson, TX 75080 USA (e-mail: wooram.park@utdallas.edu).

G. S. Chirikjian is with the Department of Mechanical Engineering, Johns Hopkins University, Baltimore, MD 21218 USA (e-mail: gregc@jhu.edu).

Color versions of one or more of the figures in this paper are available online at <http://ieeexplore.ieee.org>.

Digital Object Identifier 10.1109/TASE.2013.2295398

prealignment inherently results in imperfect alignment because of the background noise on the images, the statistical information of the imperfect alignment can be obtained and is used for the iterative CC at the next step to obtain better alignment at the end. Since the prealignment involves the principal axes of images, the alignment method proposed in this paper targets the alignment of non-circular projection images.

Index Terms—Class averages, cross correlation (CC) algorithm, image alignment, single-particle electron microscopy (EM).

I. INTRODUCTION

THE MAIN theme of this paper is that using probability densities in planar pose, including both position and orientation, of projected images of highly anisotropic particles in cryo electron microscopy (EM) adds value to existing image alignment methods which suppress the dependence on orientation. This introduction section consists of four subsections. Section I-A reviews single-particle EM and class averaging in single-particle EM. Section I-B reviews the existing image alignment methods for class averaging in single-particle EM. Section I-C reviews how pose densities are used in the fields of Simultaneous Localization and Mapping (SLAM) and Assembly Automation. Section I-D explains how the concept of pose densities can be connected to image alignment in order to improve a conventional method.

A. Class Averaging in Single-Particle Electron Microscopy

The main goal of single-particle EM is to reconstruct three-dimensional structural density of bio-macromolecules (and complexes formed from multiple molecules) from noisy planar projections obtained from a transmission electron microscope, as shown in Fig. 1. This structural information leads to better understanding of the function and mechanisms of bio-macromolecular complexes. Since intensive computation is required for preprocessing of a high volume of images and the three-dimensional reconstruction, partially or fully automated algorithms for the image processing and the reconstruction have been pursued extensively. Several widely used computational packages have been developed for this purpose (e.g., EMAN [2], SPIDER [3], IMAGIC [4], and XMIPP [5]).

In experiments, many essentially identical copies of a bio-macromolecule of interest are embedded in a thin support layer. Depending on the experimental techniques, the method of specimen preparation varies. In cryo electron microscopy, the support layer for the bio-macromolecule consists of vitrified buffer made by flash-freezing a solution. In the negative staining technique, the support layer consists of a dense metallic salt, and

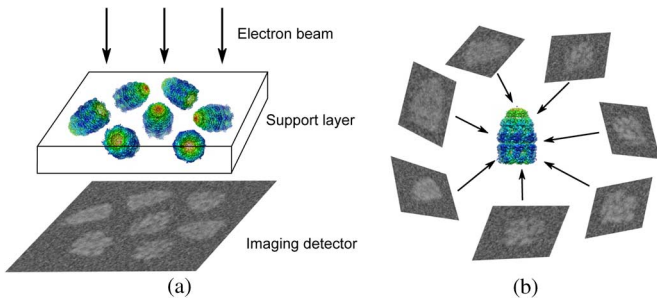


Fig. 1. Scheme of single-particle electron microscopy. (a) The electron microscope takes the projections of identical and randomly oriented macromolecules. (b) The three-dimensional structure is reconstructed from many two-dimensional electron micrographs.

the density of the bio-macromolecules is lower than the surrounding. The main reason that the projections are taken from multiple molecules instead of a single molecule is because it is hard to obtain multiple projections from a single molecule due to the damage to the molecular structure resulting from high-energy electrons. In the traditional setup for single-particle electron microscopy, as shown in Fig. 1, each molecule is exposed to the electron beam only once, and natural randomness in the orientations of these essentially identical molecular structures is used to generate projections in different directions relative to the body frame of a representative structure. This is an alternative to a tilt series consisting of many projections of a single molecule through directions that are *a priori* known relative to each other.

Suppose that the support layer is in the horizontal plane, and an electron beam takes projections of the structural density of the embedded bio-macromolecules along the vertical direction. In principle, the three-dimensional shape of the bio-macromolecules can be reconstructed using these projection images. Although this reconstruction is very similar to computed tomography, there is the obvious difference that the projection angles are unknown *a priori* and the higher dimension is considered in reconstruction in electron microscopy.

The existing pipeline for the overall process of single-particle electron microscopy is shown in Fig. 2. There are opportunities for automation at each stage. For example, in the steps of image collection and refinement in Fig. 2, a method to detect images containing particle projection can be used [6], and a denosing method can reduce the noise in electron micrographs [7]. In addition, there are commercial products such as the Vitrobot [8] that can be used for vitrification preparation. In this paper, we focus on algorithms for automated image refinement based on joint probability densities in position and orientation. Though such probability densities are common in SLAM and Assembly Automation, the orientational dependence is typically suppressed in image alignment methods used in single-particle electron microscopy.

As a general principle, crosscutting approaches tend to enrich those fields that they touch. In this light, the development of algorithms for structural biology may benefit from concepts that originate in the field of automation engineering. The former is a scientific subfield of biology, whereas the latter originates in engineering. As interdisciplinary approaches become more popular, and the techniques and perspectives from one area are

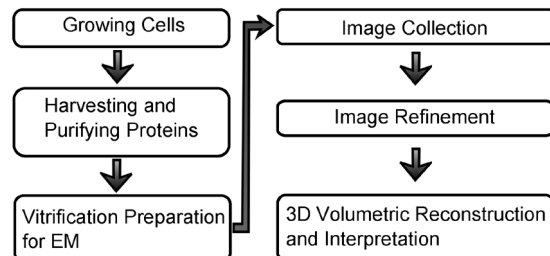


Fig. 2. The pipeline for protein structure determination using single-particle electron microscopy.

more readily accepted in another, the potential exists for both to benefit.

In electron microscopy with bio-macromolecules, the electron dose is limited to reduce structural damage on the specimen by high-energy electrons. This leads to an extremely low signal-to-noise ratio (SNR) in electron micrographs [9]. One conventional approach to deal with the low SNR images is to consider a *class* of images corresponding to the same (or quite similar) projection direction. Each image in a class can be thought of as the sum of the same clear projection of the three-dimensional structure and a random background noise field. A *class average* is the representative image for each class. During the averaging process, the additive background noise is reduced and the resulting average is a high SNR image and is believed to be close to the clear projection. Prior to the class averaging, an alignment is required to estimate the pose (position and orientation) of the underlying projection in each image. Needless to say, more accurate and faster algorithms for alignment will result in better reconstruction results.

Many algorithms for three-dimensional reconstruction using electron microscopy iteratively refine an initial three-dimensional density [2]–[5], [10]. The process consists of many steps, some of which are automated. First, the electron micrographs are grouped into classes. Then, the images in each class are aligned and averaged to yield characteristic views, and the projection angles of each view are computed [9]. Once an initial three-dimensional density is reconstructed, the steps of classification, alignment, averaging, projection angle assignment, and three-dimensional reconstruction are iterated to convergence, to yield a final density. Image alignment is an important step for the averaging and structure refinement. The accuracy and efficiency of the alignment can therefore affect the overall performance of the three-dimensional reconstruction process.

B. Review of EM Image Alignment

This paper focuses on a method for image alignment in single-particle EM. Accurate alignment is an important step in the whole reconstruction problem in single-particle EM. A brief review of existing methods for EM image alignment is given next.

The cross correlation (CC) method is one of the most popular computational tools for the EM image alignment [11]. The maximum CC occurs at the best alignment of two images. However, if the SNR of images is low, false peaks in the CC function degrade the accuracy of the CC method. More recently, Penczek *et al.* [12] proposed a new alignment method

using nonuniform FFT. They used a gridding method to resample images with high accuracy, and then found a better alignment for the images. The computational efficiency of various alignment methods was also investigated in [13].

Typically, the CC method for alignment of electron micrographs is implemented as an iterative process and requires an initial guess for the underlying intrinsic image. Due to this requirement, users should intervene in the computational process. If the preliminary structural information (e.g. symmetry, low-resolution features, etc.) of the biological complex of interest is given, it is relatively easy to choose the initial image for the iteration. However, this is not the case if the biological complex is being studied for the first time. Moreover, even if some preliminary information about the structure is given, it is still a hard problem to choose the best starting image. In addition, all other things being equal, a method that does not require human intervention is inherently better than one that does.

In the conventional CC method, all possible alignments are searched. In other words, the CC of two images is computed as a function of relative translations and rotations, and then the optimal alignment maximizing the CC is chosen. To search the optimal translation, the DFT is a useful and fast tool [11], [13]. However, to search the optimal rotation, an image is actually rotated by every possible rotation angle, and then the CC with the other image is computed. For an asymmetric projection image, a search of angles from 0 to 2π is required. In addition, limited resolution due to discretization of angles is inevitable. Since the rotation involves computationally expensive interpolation, a fine discretization increases computation time.

Penczek *et al.* [11] proposed a reference-free alignment algorithm. It consists of two steps: 1) “random approximation” of the global average and 2) refinement with the result from the first step. In the first step, images are sequentially aligned and averaged in randomized order. In the second step, the alignment for each image from the first step is improved so that each image is best aligned to the average of the rest of images. Marco *et al.* [14] modified the first step to reduce the effect of the order of input images. They proposed a prealignment method based on a pyramidal structure, instead of the sequential alignment. All the images are paired, aligned and averaged. Then, the same process is repeated with the resulting images until one image remains.

An alternative to the CC approach is the maximum-likelihood (ML) method developed in [15]. This method does not directly find the alignment for each image in a class. Rather it finds the underlying projection using statistical models for the background noise and the pose of the projection. The likelihood is defined as a function of the projection image and the parameters for the statistical models. The *refinement* process finds the projection image and the parameters by maximizing the likelihood function. This approach has been extended to deal with the case where data images of a class are heterogeneous [16]. It was shown that the ML method outperformed the CC method [15].

C. Applicable Methodologies From SLAM and Assembly Automation

In this paper, we pay attention to an analogy between: (1) problems in robotics and assembly automation and (2) the alignment of anisotropic projection images in single-particle

cryo-EM. Although (1) involves the distribution and manipulation of physical parts and (2) involves the manipulation of images, a common feature in both problems is the use of probability densities in position and orientation (or pose, for short). We show that methods familiar in addressing (1) may provide an opportunity to add new perspectives in (2). We provided a brief review of the existing pipeline for automated protein structure determination using single-particle EM. We did this to help readers who work on (1) and may not have prior knowledge of (2) to understand where the algorithms developed here can fit in this pipeline.

In the subfield within Robotics known as SLAM, time-varying probability density functions (pdfs) of the form $f(x, y, \theta; t)$ are used to update probabilistic estimates of pose of the mobile robots that move in the plane [17]–[20]. The temporal evolution of the pose pdf is based on a combination of noisy models of locomotion (such as dead reckoning estimates resulting from integrating nonholonomic kinematics) and noisy sensor measurements. These probabilities can be computed either by sampling methods (as described in the references above), or using closed-form expressions as described in [21]–[23]. Three-dimensional pose distributions and SLAM problems arise in the context of vehicles moving over rugged terrain, quad-copters, and 3D manipulation [24]–[26], as well as in the steering of flexible needles [27]–[30].

In the field of Assembly Automation, practical rules for orienting parts to within quantitatively evaluated tolerances using provably correct algorithms have long been known [31]–[36]. Moreover, the analysis of symmetry in parts and the resulting symmetry induced in pose distributions has been studied in [37] and [38], with an eye towards the design of robotic systems capable of self-diagnosis, self-repair, and self-replication [39]–[41].

Whereas computations involving probabilities in pose are now very common in SLAM and Assembly Automation, they are not widely used in processing of EM images. Therefore, one of the goals of this paper is to illustrate how these methods can be applied to this problem, thereby opening new connections between these fields.

D. Overview of Methods and Organization of This Paper

This paper focuses on a method for image alignment before image averaging that was explained in Section I-A. Our method is particularly well suited to nonspherical particles such as ion channels. The projections of these non-spherical particles are typically noncircular, leading us to investigate how to exploit this anisotropy to improve existing class-averaging algorithms.

Inspired by the use of probability density functions in pose for SLAM problems, we explore a modification to the CC method for nonspherical particles that significantly improves its performance by exploiting the orientational tendency of images. Namely, we prealign classified images and then apply the CC method to realign the class images.¹ Using the alignment method in [1], the images are coarsely aligned by matching the centers of mass and the principal axes of images. The second step (realignment) uses the resulting average, the alignment

¹We assume that an initial classification is made by an existing algorithm such as EMAN [2]. Recent *classification-free* methods presented in [42] are another possible alternative to existing algorithms.

for each image, and the distribution of misalignment from the first step (prealignment). The most important benefit of this prealignment is that we can estimate the pose distribution of the misalignment. This distribution enables us to reduce the search space for the CC method to those poses that are most probable. Since the search space is reduced, the sampling interval is also reduced for a fixed number of samples. In addition, this prealignment process automatically produces a reference image which is used for the next iterative realignment. Therefore, the user does not have to provide a reference image, which increases the autonomy of the algorithm. Using synthetic data images, we will show how our new method improves the conventional CC method.

The remainder of this paper is organized as follows. In Section II, we review the CC method for class averaging in single particle electron microscopy. In Section III, we propose a new method to better align very noisy images using a pose distribution of misalignment that has a closed analytical form. In Section IV, the results obtained by the new and existing methods are presented and the resulting images are assessed using several measurement methods. Finally, the conclusion is presented in Section V.

II. MATHEMATICS OF THE CROSS CORRELATION METHOD

A class average can be defined as

$$\gamma(\mathbf{x}) = \frac{1}{N} \sum_{i=1}^N \rho_i (g_i^{-1} \cdot \mathbf{x}) \quad (1)$$

where $\rho_i(\mathbf{x})$ is the i th image in a class and $g_i = g(\mathbf{q}_i)$ represents the planar rigid-body motion responsible for alignment of the image with roto-translation parameters $\mathbf{q}_i = (q_{\theta_i}, q_{x_i}, q_{y_i})$. In this context, each rigid-body transformation such as g_i can be thought of as a particular evaluation of the matrix-valued function $g(\mathbf{q})$ defined as

$$g(\mathbf{q}) = \begin{pmatrix} \cos q_\theta & -\sin q_\theta & q_x \\ \sin q_\theta & \cos q_\theta & q_y \\ 0 & 0 & 1 \end{pmatrix}. \quad (2)$$

Moreover, each g_i performs the “action,” \cdot of moving a point in the plane, $\mathbf{x} \in \mathbb{R}^2$. Specifically, the action, \cdot in (1) is achieved by multiplication of the matrix (g_i^{-1}) and the vector (\mathbf{x}) inside the function, which has the effect of moving the function by g_i .

The optimal alignment can be obtained by maximizing the following quantity [11]:

$$C(g_1, \dots, g_N) = \int_{\mathbb{R}^2} \left[\sum_{i=1}^N \rho_i (g_i^{-1} \cdot \mathbf{x}) \right]^2 d\mathbf{x}. \quad (3)$$

It was shown in [15] that this problem can be solved using iterative optimization. After the n th iteration, the next iteration result is given as [15]

$$g_i^{(n+1)} = \arg \max_g \left(\rho_i(g^{-1} \cdot \mathbf{x}) \odot \left[\gamma^{(n)}(\mathbf{x}) - \frac{1}{N} \rho_i(g^{-1} \cdot \mathbf{x}) \right] \right) \quad (4)$$

where \odot denotes the inner product between two image arrays, such that

$$A \odot B = \sum_{k,l} a_{kl} b_{kl}$$

and $\gamma^{(n)}$ is computed using (1) with $g_i^{(n)}$ in place of g_i . Explicitly, using the improved alignment $g_i^{(n+1)}$, the averaged image is refined as

$$\gamma^{(n+1)}(\mathbf{x}) = \frac{1}{N} \sum_{i=1}^N \rho_i \left(\left[g_i^{(n+1)} \right]^{-1} \cdot \mathbf{x} \right). \quad (5)$$

To find the maximizer in (4), the CCs for possible alignments (translations and rotations) are computed and the maximizer is chosen. Each image is actually rotated by candidate rotation angles and the CC of the two images are computed as a function of translation. This can be easily implemented using the DFT. For various rotation angles, we stack the CC, and the three-dimensional search for the maximum CC gives the optimal alignments. This alignment method is referred to as *direct alignment using 2D FFT* in [13].

The image rotation of discrete images requires interpolation. Since every class image should be rotated several times by possible rotation angles, the computation time for the whole class images is considerable. There is a tradeoff between the computation time and the accuracy of the result. In addition, the CC method may fail with low SNR images because of the existence of false peaks in the CC.

As shown in (4), the iteration process in the CC method requires a reference as a starting image. Explicitly, an initial reference $\gamma^{(0)}$ is required to get the first alignment $g_i^{(1)}$ in (4). After this, the iteration of (4) and (5) will converge to the resulting alignment and average image. Even though a reference-free alignment method is available [11], it is essentially a two-step method; the first step generates a reference image out of data images and then the second step refines the reference iteratively. In addition to the issue about reference images, the CC is computed for various alignments to find the maximum CC. A finer discretization for the rotation angles may yield better accuracy, but this comes at the cost of increased computation time.

III. METHODS

The new method proposed in this paper consists of two parts: prealignment of class images and application of the CC method to the prealigned images with blurring and segmentation.

A. Matching Centers of Mass and Principal Axes of Images

Matching centers of mass and principal axes (CMPA) of two images gives the alignment of a class of images [1]. The accuracy of the alignment by this method is sensitive both to the background noise and the degree of circularity of the underlying pristine projection. However, the advantage of this alignment method is that we can estimate the distribution of the misalignments. This provides a better starting point than assuming a uniform orientation distribution.

As derived in [1], the probability density function for the misalignments after the CMPA matching is given as²

$$p(q_x, q_y, q_\theta; \xi_\sigma, \xi_\theta) = \frac{1}{2\pi\xi_\sigma^2} e^{-\left(\frac{q_x^2+q_y^2}{2\xi_\sigma^2}\right)} \times \frac{1}{2\sqrt{2\pi}\xi_\theta} \sum_{k=-\infty}^{\infty} \left(e^{\frac{-(q_\theta-2\pi k)^2}{2\xi_\theta^2}} + e^{\frac{-(q_\theta-(2k+1)\pi)^2}{2\xi_\theta^2}} \right). \quad (6)$$

While the misalignments of translation forms a unimodal Gaussian distribution, the misalignments of rotation forms a bimodal distribution. This is because an image has two equivalent principal axes whose directions are opposite to each other. Though this ambiguity makes it difficult to determine the rotational alignment, it is easy to have the resulting distribution for the rotational misalignment. It is essentially the average of two Gaussian functions wrapped around the circle with the same standard deviation ξ_θ and two different means, 0 and π . For $N \times N$ images, the parameters in (6) are computed directly from the background noise properties as [1]

$$\xi_\sigma = \sqrt{K \sum_{l=1}^N x_l^2} \quad (7)$$

$$\xi_\theta = \sqrt{\frac{K}{(\lambda_1 - \lambda_2)^2} \left(K \sum_{l=1}^N x_l^2 \sum_{k=1}^N y_k^2 + \sum_{l=1}^N x_l^2 y_l^2 \right)} \quad (8)$$

where $x_l = y_l = l - (N+1)/2$, $K = (1+4\nu)\sigma^2/M^2$, σ^2 is the variance of the background noise, and ν is the correlation coefficient between the noise in adjacent pixels. M is defined as $M = (1/N) \sum_i \sum_j \rho_i(\mathbf{x}_j)$, which is the mean of the sum of the pixel values of images. The sums in (7) and (8) can be simplified as closed-form expressions as

$$\xi_\sigma = \sqrt{\frac{K}{12} N(N^2 - 1)}$$

$$\xi_\theta = \frac{\sqrt{K}}{(\lambda_1 - \lambda_2)} \times \sqrt{\left(\frac{K}{144} N^2 (N^2 - 1)^2 + \frac{N}{240} (3N^2 - 7)(N^2 - 1) \right)}.$$

The inertia matrix of an image aligned by matching CMPA is computed as

$$J_i = \frac{1}{M} \sum_j \mathbf{x}_j \mathbf{x}_j^T \rho'_i(\mathbf{x}_j) = \begin{pmatrix} L_x(i) & 0 \\ 0 & L_y(i) \end{pmatrix}.$$

Note that the image $\rho'_i(\mathbf{x}_i)$ is a rotated version of $\rho_i(\mathbf{x}_i)$ which is aligned so as to have a diagonal inertia matrix. The term $(\lambda_1 - \lambda_2)$ in (8) is defined as

$$(\lambda_1 - \lambda_2) = \frac{1}{N} \sum_i (L_x(i) - L_y(i)).$$

²In that paper, a method for resolving the 180° ambiguity in principal-axis alignment was also provided to make the resulting orientational distribution unimodal in cases of relatively high SNR (e.g., 0.2 and higher). However, this symmetry-breaking fails for the case of low SNR (e.g., 0.05 and lower) and the statistical characterization of this in a way that can be used in CC is nontrivial, and so the version of $p(\cdot; \cdot)$ used here is bimodal.

Consequently, we can easily characterize the alignment error which the specific alignment method (the CMPA matching) produces, while general approaches to compute the alignment error in data images were developed in [43] and [44].

Note that as $|\lambda_1 - \lambda_2| \rightarrow 0$, as would be the case for a circular image, $\xi_\theta \rightarrow \infty$, and the folded normal reduces to the uniform distribution on the circle. This may not be obvious from the form given in (6), but by writing this same orientational distribution in the form of a Fourier series as is done in [45, Eq. 2.46], the convergence to uniformity as ξ_θ becomes infinite becomes obvious. Hence, the method used here is general, though the value that it adds to the existing literature is realized when the projections are anisotropic and hence the smaller ξ_θ is, the more useful our approach becomes.

Due to the fact that the misalignment distribution after the CMPA matching can be modeled by (6) and the model parameters are computed as (7) and (8) regardless of the characteristics of preexisting misalignment, our method with the CMPA matching has benefits compared to the ML method in [15]. The ML method assumes the Gaussian model and uniform distribution for the image misalignment in translation and rotation, respectively. The model parameters are also estimated iteratively during the refinement process in the ML method. The whole process takes longer because of the model parameter estimation that is embedded in the iteration. In addition, the ML method will fail if the image misalignment does not follow the assumed distribution model. In our method, the CMPA matching process will erase the preexisting statistical characteristics of the image misalignment, and after the matching process, the image misalignment should follow the Gaussian distribution in (6) and the parameters are directly computed as (7) and (8).

This matching algorithm has one more benefit compared to the reference-free alignment in [11] and [14]. In the CMPA matching method, each image can be aligned independently, while two images should be considered to align in [11] and [14]. Essentially, we align images to a reference frame in the CMPA matching. In other words, the center of mass and the principal axis of a image are matched to a space-fixed reference frame rather than pairwise between images. Therefore, the alignment result is independent of the order in which we consider the input images. In contrast, the first step of the reference-free method in [11] is dependent on the input order. Even though Marco *et al.* [14] developed an alternative method which is less sensitive to the input order, it is not completely independent of the order of input images. Consequently, our method generates the consistent result regardless of the order of the input images, while the results from previous approaches in [11] and [14] may vary depending on the input order.

Obviously, with high SNR images, matching the CMPA of images will generate accurate alignment. In this case the misalignment can be removed from a blurry class average using a deconvolution technique [46]. For low SNR images, we will apply a new method which we propose in the next subsection.

B. Modified Cross Correlation Method

1) *Search Space for Alignment:* As seen in Section III-A, the statistics of misalignments after the CMPA matching can be

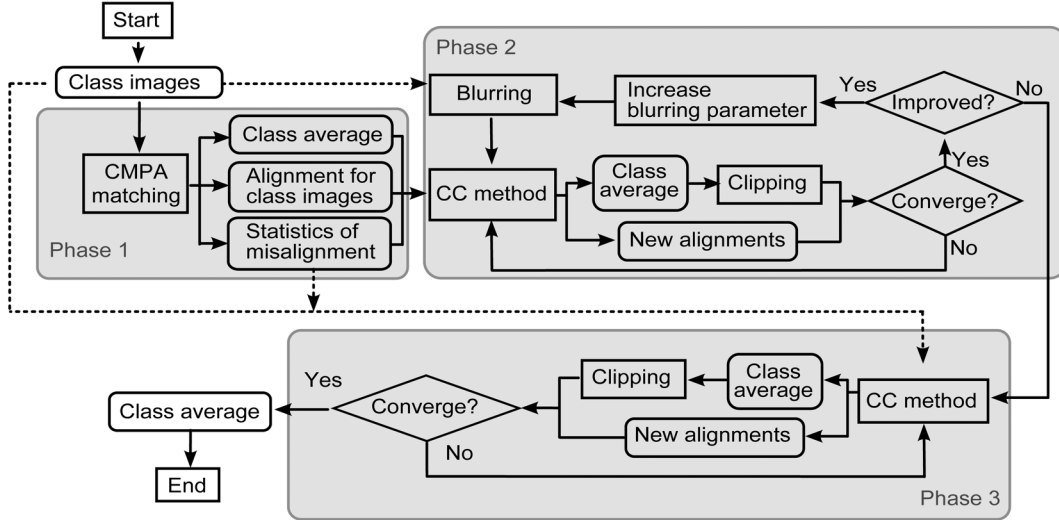


Fig. 3. Diagram for the new alignment method.

modeled using Gaussian functions with the parameters defined in (7) and (8).

This reduces the search space. Without the CMPPA matching approach, the search space for rotation would be $[0, 2\pi)$ and the sampling interval should be equally spaced because there is no information about the tendency of orientation. However, after we prealign images using the CMPPA matching, the rotation angles associated with the misalignment are distributed around the values 0 and π with the computed standard deviation. Thus, we can focus on a smaller search space for the realignment. Furthermore, the sampling interval should be designed according to the distribution. This sampling can be performed using inverse transform sampling. A sample value X is obtained as

$$X = F_c^{-1}(Y)$$

where F_c is the cumulative distribution function of the normal distribution and Y is drawn from a uniform distribution on $(0, 1)$. In practice, we use the equally spaced value from $(0, 1)$ for Y to reduce the ambiguity that the random values for Y may produce.

2) Image Blurring and Segmentation: As is widely known, the CC method exhibits false peaks for low SNR images. To avoid false maxima, we artificially blur the images during the early iterations of the CC method. Practically, we convolve data images with a two-dimensional Gaussian to generate the blurred version of the images. The method to choose the optimal blurring parameter will be proposed in Section III-C (see Phase 2 in Fig. 3).

Since class images contain one projection of a single particle, we can expect that there are two regions in the image: projection image region and pure noise region. When we apply the CC method, the background noise in the intermediate average [$\gamma^{(n)}(\mathbf{x})$ in (4)] degrades the performance of the CC method. This noise in the pure noise region can be eliminated by a image segmentation technique, because it is easier to distinguish the projection region and the pure noise region in the intermediate average. We apply the edge detection algorithm developed in [47] to solve this segmentation problem.

3) Successive Transformations: The new method proposed here consists of the prealignment by CMPPA matching and the realignment by the iterative CC method with the reduced search space. During the process, each image will be repeatedly transformed (rotation and translation) to find the best alignment. If we apply multiple transformations (rotations and translations) on a two-dimensional discrete image successively, the resulting image will have many artifacts since such transformations of digital images involve interpolation. To overcome this, instead of storing the transformed images for the next iteration, we record the transformation information for each image maintaining the original images. Two consecutive rigid body transformations on the plane result in one combined transformation. The combined transformation can be computed using the rigid body motion group which is one popular mathematical tool in robotics [48].

Two 3×3 matrices representing pure rotation and pure translation on the plane can be, respectively, written using (2) as

$$g_r(\theta) = \begin{pmatrix} R(\theta) & \mathbf{0} \\ \mathbf{0}^T & 1 \end{pmatrix} = g(\theta, 0, 0)$$

and

$$g_t(\mathbf{p}) = \begin{pmatrix} I & \mathbf{p} \\ \mathbf{0}^T & 1 \end{pmatrix} = g(0, p_1, p_2)$$

where

$$R(\theta) = \begin{pmatrix} \cos \theta & -\sin \theta \\ \sin \theta & \cos \theta \end{pmatrix}$$

$\mathbf{0}$ is the 2D zero vector, and $\mathbf{0}^T$ is its transpose. $g_r(\theta)$ and $g_t(\mathbf{p})$ represent pure rotation and pure translation in the plane, respectively.

If we translate and then rotate an image respectively by \mathbf{p} and θ relative to the frame of reference fixed at the origin, then the resulting transformation is written as

$$g^*(\theta, \mathbf{p}) = g_r(\theta)g_t(\mathbf{p}) = \begin{pmatrix} R(\theta) & R(\theta)\mathbf{p} \\ \mathbf{0}^T & 1 \end{pmatrix}.$$

Two successive transformations, $g^*(\theta_1, \mathbf{p}_1)$ followed by $g^*(\theta_2, \mathbf{p}_2)$, can be written as:

$$\begin{aligned} & g^*(\theta_2, \mathbf{p}_2)g^*(\theta_1, \mathbf{p}_1) \\ &= \begin{pmatrix} R(\theta_2)R(\theta_1) & R(\theta_2)R(\theta_1)\mathbf{p}_1 + R(\theta_2)\mathbf{p}_2 \\ \mathbf{0}^T & 1 \end{pmatrix} \\ &= \begin{pmatrix} R(\theta_2)R(\theta_1) & \mathbf{0} \\ \mathbf{0}^T & 1 \end{pmatrix} \begin{pmatrix} I & \mathbf{p}_1 + R(-\theta_1)\mathbf{p}_2 \\ \mathbf{0}^T & 1 \end{pmatrix} \quad (9) \end{aligned}$$

Therefore, the successive transformations can be viewed as the translation by $\mathbf{p}_1 + R(-\theta_1)\mathbf{p}_2$ followed by the rotation by $(\theta_1 + \theta_2)$. Note that all the transformations here are performed using the fixed frame of reference attached to the center of the bounding box.

Combined with the reduced search space, this tool enables a search with finer alignment angles. In the conventional CC method, only the predefined discrete angles are considered. Specifically, each class image is eventually assigned to one of the predefined discrete angles. Since the angles are equally spaced samples from $[0, 2\pi]$, the resolution of the rotational alignment is limited by $2\pi/N$, where N is the number of samples. However, in our method, the prealignment by the CMPA matching gives the statistically determined alignment angles and the candidate alignment angles for realignment are sampled within a smaller and more targeted search space guided by the knowledge of the mean and variance of the CMPA. During the iteration, the realignment information for each image is obtained and then the new combined transformation is computed using the previous alignment information and the new alignment information. We do not store the transformed images, rather store the alignment information keeping the original class images. Using this manipulation, we can avoid the image artifacts that may be caused by multiple transformations.

C. Flow of the New Method

The flow chart for the new alignment method is shown in Fig. 3. The rectangles and the rounded rectangles in black denote operations and data, respectively. The continuous lines with arrows denote the main flow of the new method. The dotted lines with arrows describe that the original images are used in the subroutines.

In Phase 1, the images are coarsely aligned by matching the CMPA of images. After this process, we have the alignment for every image, an averaged image, and the statistical information about misalignment involved in the coarse alignment.

In Phase 2, we first blur the images from Phase 1 using a Gaussian kernel. We start with the standard deviation 0.25 pixel for the Gaussian kernel. Then, we apply the CC method to realign the blurred image. The iterative process in Phase 2 takes the averaged image from Phase 1 as a reference image. Also, the reduced search space for alignments based on the distribution of misalignment is applied. This iteration is repeated until it converges with 3% threshold. In other words, this iteration will stop when the image improvement measured by the normalized least-square error (NLSE) is less than 3%. After this iteration denoted by the lower loop in Phase 2 in Fig. 3, we compute the cost function (3) to measure the effectiveness of the artificial blurring. We repeat the lower loop iteration in Phase 2 with the

TABLE I
SIGNAL-TO-NOISE RATIOS AND CORRELATIONS OF THE ADJACENT NOISE PIXELS FOR TWO TEST CASES

	Case 1	Case 2
SNR	0.025	0.100
Correlation	0.0	0.3

increased blurring parameters until we find the optimal blurring parameter. The parameter is increased by 0.25 pixel for each step. This simple search for the blurring parameter is valid because the alignments without blurring and with a large blurring will both produce bad results and the optimal blurring parameter will exist in between. The realignment in Phase 2 cannot be accurate because the blurred images are used. Even though the realignment is not satisfactory, this process gives better alignment than Phase 1 and we can avoid the problems associated with false peaks in CCs.

In Phase 3, we find more accurate alignment. This phase applies the CC method to the original version of images. The reduced search space and the resulting alignments (from Phase 2) for images play an important role in this phase. Iterations are performed until they converge.

In Phases 2 and 3, the projection region in the averaged image after each rotation is segmented and then used in order to avoid the effects of the noise surrounding the region of interest in the image on the next iteration. In addition, we do not store the rotated and translated images for the next iteration. Rather, we use the original images with their alignment information for the next iteration as denoted by the dotted lines with the arrows. This reduces the interpolation error which may occur during repeated rotation and translation of images. For given successive transformations, we can use a combined transformation from the method in Section III-B3.

IV. RESULTS

In this section, we compute the alignment and the class average for two cases defined in Table I using the new method, and then compare it to the results of the conventional CC method and the ML method.

To generate the synthetic data images, we first transform (i.e., translate and rotate) the clear projection image of GroEL/ES (PDB code: 1AON) shown in Fig. 4(a). The image size is 64×64 pixels. The rotational angles are sampled at random from a uniform distribution on $[0, 2\pi]$. The translation distances are sampled at random from a Gaussian distribution with the standard deviation, 5 pixel. After transforming, we add noise to the transformed projection. The intensity of the noise is determined so that the resulting image has the SNRs defined in Table I. The parameter ν is the correlation coefficient between the noise in adjacent pixels. The method of generating the noise with ν was introduced in [1]. Fig. 4(b) shows the class average of 500 class images with the perfect alignments for Case 1. Fig. 5 shows the noisy data images for the two cases and their blurred version which is used in Phase 2 in Fig. 3.

The search space for translation is bounded by $(-2.35\xi_\sigma, 2.35\xi_\sigma)$. The value 2.35 is the value dictated by Gaussian statistics to guarantee that 98% of the mass under the Gaussian distribution is sampled. Since the probability

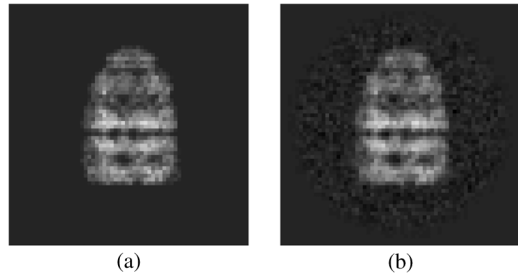


Fig. 4. (a) The original clear projection. (b) The average image with the unattainable perfect alignment for Case 1.

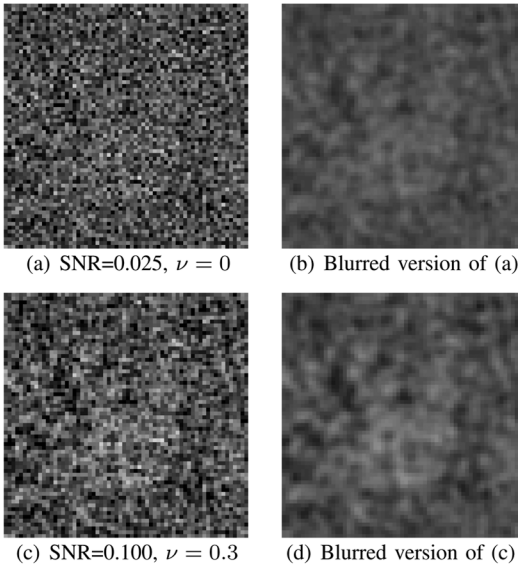


Fig. 5. (a) and (c) Example test images in Case 1 and 2, respectively. (b) and (d) The blurred version of (a) and (c), respectively. ν is the correlation between the noise in two adjacent pixels in the background. (a) SNR = 0.025, $\nu = 0$. (b) Blurred version of (a). (c) SNR = 0.100, $\nu = 0.3$. (d) Blurred version of (c).

density function for the rotational angles is bimodal, the two intervals $(-2.35\xi_\theta, 2.35\xi_\theta)$ and $(-2.35\xi_\theta + \pi, 2.35\xi_\theta + \pi)$ are searched. Note that ξ_σ and ξ_θ were given in (7) and (8). They are computed from the background noise properties, and are not adjustable parameters. The translational misalignment is limited to a multiple of one pixel length because translation by subpixel distance involves interpolation and increases the computation time without bringing new information out of images. This limited search also enables us to compute the CC using the DFT. We sample 22 angles for rotational search using the inverse transform sampling. Two sets of 11 samples are drawn from the intervals $(-2.35\xi_\theta, 2.35\xi_\theta)$ and $(-2.35\xi_\theta + \pi, 2.35\xi_\theta + \pi)$, respectively.

Fig. 6(a) shows the coarse alignment obtained by the CMPA match for Case 1. In Phase 2, we use the blurred version of class images to avoid false peaks in the CC. Even though the optimal parameter for the artificial blurring is determined as $\sigma = 0.5$ pixel if we apply the full process of Phase 2 described in Section III-C, we observe that the final result after Phase 3 is not heavily dependent on the blurring parameter when we consider $\sigma = 0.25, 0.50, 0.75$ or 1.00 pixel. For demonstration, we

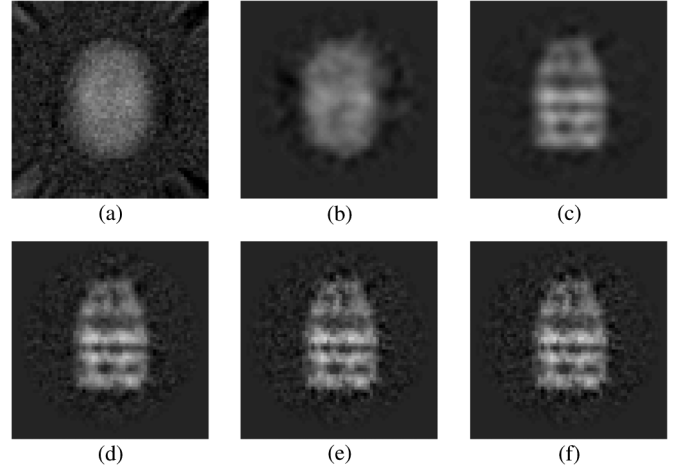


Fig. 6. The result of the new method for Case 1. (a) Result by CMPA (Phase 1). (b) Initial image for Phase 2. (c) Result of Phase 2. (d) Initial image for Phase 3. (e) Result of Phase 3. (f) Resulting image after 30 iterations.

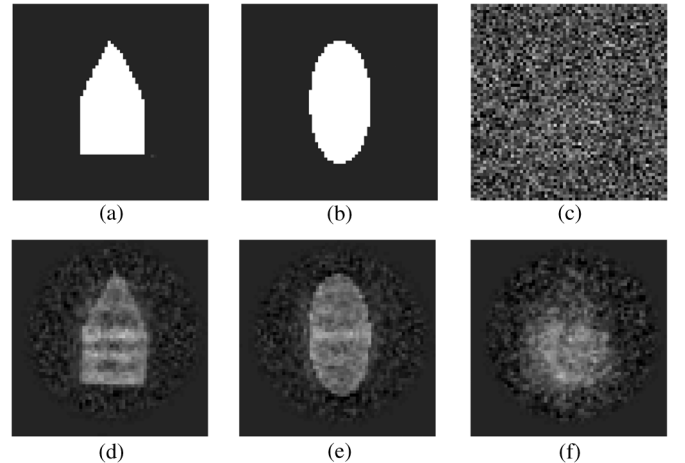


Fig. 7. The results of the conventional CC method for Case 1 with three reference images. Reference 3 is one class image. (a) Reference 1. (b) Reference 2. (c) Reference 3. (d) CC 1. (e) CC 2. (f) CC 3.

fix the standard deviation for the artificial blurring as $\sigma = 1$ pixel without losing the benefit of Phase 2. For Case 1, Fig. 6(b) shows the first iteration result in Phase 2. Next, the iteration in Phase 2 was repeated up to ten iterations [Fig. 6(c)]. From the 11th iteration [Fig. 6(d)], Phase 3 is applied until it converges. The 19th iteration [Fig. 6(e)] shows the converged result. As mentioned earlier, during iterations, the combined transformations for each image are computed and recorded.

Fig. 7 shows the results by the conventional CC method for Case 1 with three different reference images. We used 22 equally spaced samples on the interval $[0, 2\pi]$ for angles in the CC method.

To assess the results, we use Fourier ring correlation (FRC). The FRC provides the normalized CC coefficients over corresponding rings in Fourier domain [49], [50]. The FRC for two images, ρ_1 and ρ_2 , is defined as

$$\text{FRC}(r) = \frac{\sum_{\mathbf{r}_i \in r} \hat{\rho}_1(\mathbf{r}_i) \hat{\rho}_2^*(\mathbf{r}_i)}{\sqrt{\sum_{\mathbf{r}_i \in r} |\hat{\rho}_1(\mathbf{r}_i)|^2 \cdot \sum_{\mathbf{r}_i \in r} |\hat{\rho}_2(\mathbf{r}_i)|^2}}$$

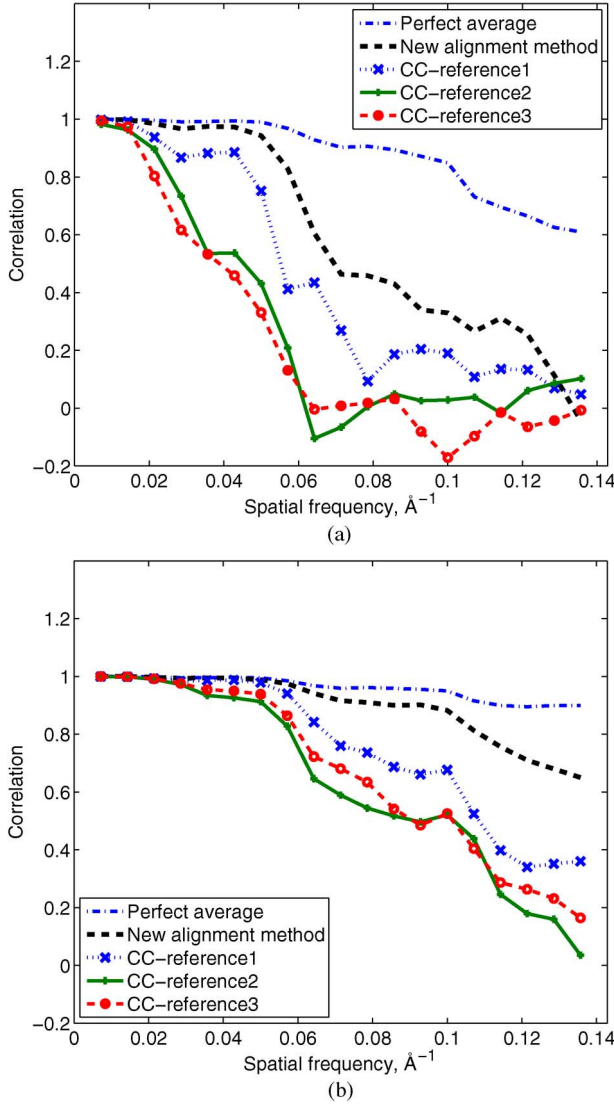


Fig. 8. FRC plots for: (a) Case 1 and (b) Case 2. Comparison of FRCs of the new method and the CC method.

where $\hat{\rho}(\mathbf{r}_i)$ is the complex structure factor at position r in Fourier space, and the $*$ denotes complex conjugate. \mathbf{r}_i is Fourier-space voxels that are contained in the ring with radius r and its thickness. The thickness 0.05 was used in this paper. The FRC is used to measure the similarity of two images in this work. For two identical images, the FRC value is “1” over the whole Fourier space.

Fig. 8(a) shows the FRC curves between the pristine projection shown in Fig. 4(a) and resulting images by our new method and the conventional CC method with various reference images. The FRC of the perfect alignment (which is impossible to obtain in practice since the baseline truth is never known *a priori*, and therefore represent an absolute upper bound on the performance of any alignment method) is also shown. Fig. 8(b) shows the FRC for Case 2. Since the FRCs measure the similarity between images, Fig. 8(a) and (b) show that the proposed method outperforms the conventional CC method.

Fig. 9(a) shows the image differences between the projection in Fig. 4(a) and resulting images obtained by our new

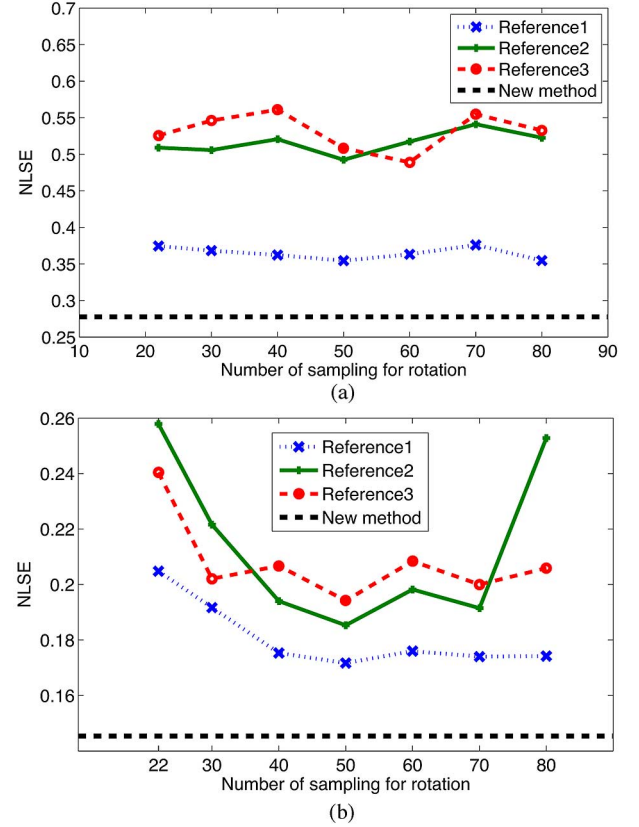


Fig. 9. Image errors measured by NLSE. The error of the proposed method (horizontal straight line) with only 22 samples for orientation is less than the other results by the CC method with more samples. (a) Case 1. (b) Case 2.

method and the conventional CC method. The differences are measured using the normalized least-square error (NLSE). The NLSE of a image $U(m, n)$ relative to another image $V(m, n)$, is defined as

$$\text{NLSE} = \sqrt{\frac{\sum_{m=1}^N \sum_{n=1}^N [U(m, n) - V(m, n)]^2}{\sum_{m=1}^N \sum_{n=1}^N [V(m, n)]^2}}.$$

The search resolution for rotational alignment becomes finer, as the number of samples is increased. Fig. 9(a) also includes the test of the conventional CC method with finer search. Specifically, the conventional CC method was applied for seven cases where 22, 30, 40, 50, 60, 70, and 80 sampling angles for rotation search were used. Interestingly, the error in Fig. 9(a) does not show the strong tendency that the result is improved as the number of samples is increased. More importantly, the results from the conventional CC method are not better than the result obtained by the proposed method with only 22 sampled angles for rotation. Note that in Fig. 9(a) the dashed horizontal line shows the error of the result obtained by the proposed method with 22 sampled angles for rotation. Fig. 9(b) also confirms that in Case 2 our method produces better result than the CC method.

When we compute the FRC and the normalized least squared errors, we align two images before computation because similarity and difference between two images are sensitive to their alignment. Since two images that we compare here are an underlying clear image and a resulting class average obtained by

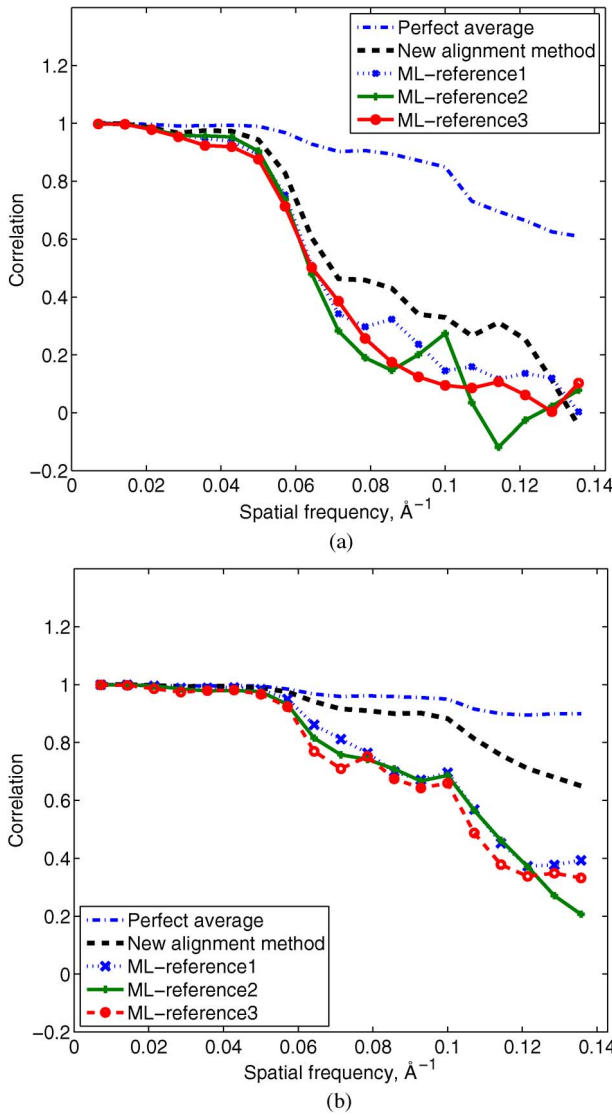


Fig. 10. FRC plots for: (a) Case 1 and (b) Case2. Comparison of FRCs of the new method and the ML method.

alignment methods, we can apply the CC method to align them without concern about false peaks in CC of noisy images. For more accurate alignment for image comparison, we also apply the image segmentation method to eliminate the area of the residual noise in the class average.

While in Fig. 8(b), the FRC curves of the results of the new method are better than those of the existing methods over all the frequency range, Fig. 8(a) shows that the curve of the result of the new method is lower than the other curves at the highest frequency. This does not mean that the resulting image of the new method is worse than the others because the curve of the result of the new method is higher at the other frequency and the image difference shown in Fig. 9(a) supports the fact that the new method produces a better image.

Even though this paper focuses on improving the conventional CC method, it is worth comparing the improved CC method and the ML method because it has been reported in the literature that the ML method generates better results than the

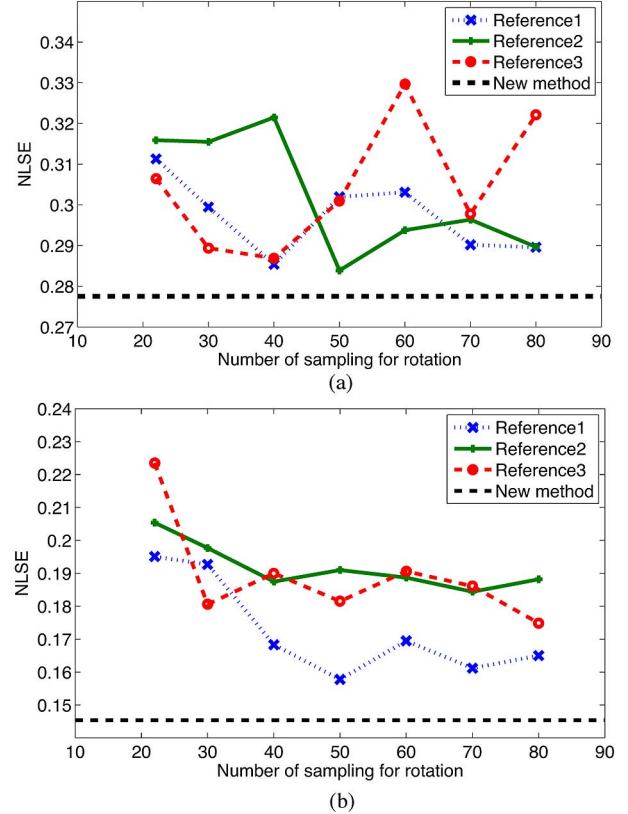


Fig. 11. Image errors measured by NLSE. The error of the proposed method (horizontal straight line) with only 22 samples for orientation is less than the other results by the ML method with more samples. (a) Case 1. (b) Case 2.

conventional CC method [15]. Fig. 10 shows that the resulting image of the new alignment method is closer to the ground truth than any results by the ML method. In addition, even if we apply the finer sampling for rotation search in the ML method, the results are not better than that of our method with coarser sampling, as shown in Fig. 11.

In the tests for the improved CC method, the conventional CC method and the ML method, we used 500 images for one class. The prealignment for the 500 images by matching CMPA took approximately 20 s using a PC (Intel Core i7 Processor 2.96 GHz, 8 MB memory) and Matlab 7.7. One iteration in Phases 2 and 3 shown in Fig. 3 took about 4.4 s. One iteration in the classical CC and ML methods takes approximately 2.6 and 6.0 s, respectively. The number of iterations until convergence in these existing methods are also shown in Table II. The total computation time of the new method for each case in Table I is about 100 s, which is less than the computation time of the ML method (150 s). The conventional CC method takes about 50 s until convergence, but the resulting images are not good as measured using FRC and normalized least squared error. It is important to note that the preprocess to compute or generate a starting reference image for the conventional CC and ML methods was not included in this computation time estimation. Therefore, the total computation times for our method and the existing methods will not be significantly different if that preprocess is counted. In addition, even if we increase the number of rotation samples for the existing methods at the expense of computation time,

TABLE II
NUMBER OF ITERATIONS FOR CONVERGENCE

	New method	CC1	CC2	CC3	ML1	ML2	ML3
Case 1	19	17	14	20	25	26	25
Case 2	17	11	16	10	26	22	28

the results are not better than that of our method with coarser sampling.

V. CONCLUSION

In this work, we developed a new alignment method for class averaging in single particle electron microscopy. The new method consists of two steps: prealignment and realignment. In the prealignment process, images in a class are aligned using their centers of mass and principal axes. Although this prealignment does not generate an accurate alignment, it provides a reasonable starting point for the next realignment process. We can quantitatively characterize the distribution of misalignments in this prealignment method. In the second step, we realign the images using the results from the first step. Essentially, we apply the CC method to realign the images from the first step with the reduced search space that was created based on the statistics of misalignment. The parametric probability densities that we use to do this are similar to those that have been used in SLAM and Assembly Planning, and are new to the microscopy application. In order to avoid problems related to false peaks in the CC method, blurred version of the images are used in the first phase of the second step. After iteration with the blurred images, we use the original image to find more accurate alignment.

We verified the proposed method using synthetic data images. We measured the Fourier ring correlation between the ground truth image and the resulting image, which quantifies the image similarity. In addition, the errors between those images were calculated to measure the difference between the ground truth and the results. In the test, we confirmed that the proposed method produces better results than the conventional CC method and the ML method. More importantly, even when the search resolution for the conventional CC method is increased at the expense of the computation time, the results of the new method were better. This validates our hypothesis that for highly anisotropic particles, the CC method is significantly enhanced by including the orientation dependence in the probability density function of the misalignments, rather than using the state-of-the-art.

The prealignment step using the CMPA matching replaces the preexisting distribution of the pose of the projection with one that is known. The statistics of misalignment can be estimated using the information about the background noise. It is worth noting that this benefit sheds new light on the ML method [15] that is based on statistics. We expect that CMPA matching can be used for the conventional ML method to make the ML method even stronger. We leave this work for future research.

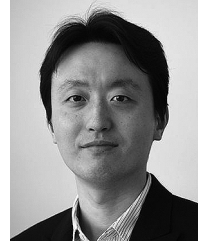
ACKNOWLEDGMENT

The authors thank Prof. F. Sigworth for providing the source code that was developed in [15].

REFERENCES

- [1] W. Park, C. Midgett, D. Madden, and G. Chirikjian, "A stochastic kinematic model of class averaging in single-particle electron microscopy," *Int. J. Robot. Res.*, vol. 30, no. 6, pp. 730–754, 2011.
- [2] S. Ludtke, P. Baldwin, and W. Chiu, "EMAN: Semiautomated software for high-resolution single-particle reconstructions," *J. Structural Biol.*, vol. 128, no. 1, pp. 82–97, 1999.
- [3] T. Shaikh, H. Gao, W. Baxter, F. Asturias, N. Boisset, A. Leith, and J. Frank, "SPIDER image processing for single-particle reconstruction of biological macromolecules from electron micrographs," *Nature Protocols*, vol. 3, no. 12, pp. 1941–1974, 2008.
- [4] M. Van Heel, G. Harauz, E. Orlova, R. Schmidt, and M. Schatz, "A new generation of the IMAGIC image processing system," *J. Structural Biol.*, vol. 116, pp. 17–24, 1996.
- [5] C. Sorzano, R. Marabini, J. Velázquez-Muriel, J. Bilbao-Castro, S. Scheres, J. Carazo, and A. Pascual-Montano, "XMIPP: A new generation of an open-source image processing package for electron microscopy," *J. Structural Biol.*, vol. 148, no. 2, pp. 194–204, 2004.
- [6] Y. Zhu, B. Carragher, R. M. Glaeser, D. Fellmann, C. Bajaj, M. Bern, F. Mouche, F. Haas, R. J. Hall, and D. J. Kriegman, "Automatic particle selection: Results of a comparative study," *J. Structural Biol.*, vol. 145, no. 1, pp. 3–14, 2004.
- [7] W. Jiang, M. L. Baker, Q. Wu, C. Bajaj, and W. Chiu, "Applications of a bilateral denoising filter in biological electron microscopy," *J. Structural Biol.*, vol. 144, no. 1, pp. 114–122, 2003.
- [8] FEI, Vitrobot, 2010. [Online]. Available: <http://www.fei.com>
- [9] J. Frank, *Three-Dimensional Electron Microscopy of Macromolecular Assemblies: Visualization of Biological Molecules in Their Native State*. New York, NY, USA: Oxford Univ. Press, 2006.
- [10] L. Wang and F. Sigworth, "Cryo-EM and single particles," *Physiology*, vol. 21, no. 1, pp. 13–18, 2006.
- [11] P. Penczek, M. Radermacher, and J. Frank, "Three-dimensional reconstruction of single particles embedded in ice," *Ultramicroscopy*, vol. 40, no. 1, pp. 33–53, 1992.
- [12] Z. Yang and P. Penczek, "Cryo-EM image alignment based on nonuniform fast Fourier transform," *Ultramicroscopy*, vol. 108, no. 9, pp. 959–969, 2008.
- [13] S. Shen, N. Michael, and V. Kumar, "Autonomous multi-floor indoor navigation with a computationally constrained MAV," in *Proc. IEEE Int. Conf. Robot. Autom. (ICRA)*, 2011, pp. 20–25.
- [14] S. Marco, M. Chagoyen, L. de la Fraga, J. Carazo, and J. Carrascosa, "A variant to the "random approximation" of the reference-free alignment algorithm," *Ultramicroscopy*, vol. 66, no. 1–2, pp. 5–10, 1996.
- [15] F. Sigworth, "A maximum-likelihood approach to single-particle image refinement," *J. Structural Biol.*, vol. 122, no. 3, pp. 328–339, 1998.
- [16] S. Scheres, M. Valle, R. Nuñez, C. Sorzano, R. Marabini, G. Herman, and J. Carazo, "Maximum-likelihood multi-reference refinement for electron microscopy images," *J. Molecular Biol.*, vol. 348, no. 1, pp. 139–149, 2005.
- [17] H. F. Durrant-Whyte, *Integration Coordination and Control of Multi-Sensor Robot Systems*. Norwell, MA, USA: Kluwer, 1987.
- [18] J. Manyika and H. Durrant-Whyte, *Data Fusion and Sensor Management: A Decentralized Information-Theoretic Approach*. Englewood Cliffs, NJ, USA: Prentice-Hall, 1995.
- [19] A. I. Mourikis and S. I. Roumeliotis, "On the treatment of relative-pose measurements for mobile robot localization," in *Proc. IEEE Int. Conf. Robot. Autom., ICRA'06*, 2006, pp. 2277–2284.
- [20] S. Thrun, W. Burgard, and D. Fox, *Probabilistic Robotics*. Cambridge, MA, USA: MIT Press, 2005, vol. 1.
- [21] Y. Zhou and G. S. Chirikjian, "Probabilistic models of dead-reckoning error in nonholonomic mobile robots," in *Proc. IEEE Int. Conf. Robot. Autom., ICRA'03*, 2003, vol. 2, pp. 1594–1599.
- [22] W. Park, Y. Liu, Y. Zhou, M. Moses, and G. S. Chirikjian, "Kinematic state estimation and motion planning for stochastic nonholonomic systems using the exponential map," *Robotica*, vol. 26, no. 4, pp. 419–434, 2008.
- [23] A. Long, K. Wolfe, M. Mashner, and G. Chirikjian, "The banana distribution is gaussian: A localization study with exponential coordinates," in *Proc. Robot. Sci. Syst.*, 2012.
- [24] A. Nüchter, *3D Robotic Mapping: The Simultaneous Localization and Mapping Problem With Six Degrees of Freedom*. New York, NY, USA: Springer, 2009, vol. 52.
- [25] S. Shen, N. Michael, and V. Kumar, "3d estimation and control for autonomous flight with constrained computation," in *Proc. IEEE Int. Conf. Robot. Autom., Shanghai, China*, 2011.
- [26] J. Kwon, M. Choi, F. C. Park, and C. Chun, "Particle filtering on the Euclidean group: Framework and applications," *Robotica*, vol. 25, no. 6, pp. 725–737, 2007.

- [27] W. Park, J. S. Kim, Y. Zhou, N. J. Cowan, A. M. Okamura, and G. S. Chirikjian, "Diffusion-based motion planning for a nonholonomic flexible needle model," in *Proc. IEEE Int. Conf. Robot. Autom., ICRA'05*, 2005, pp. 4600–4605.
- [28] R. Alterovitz, A. Lim, K. Goldberg, G. S. Chirikjian, and A. M. Okamura, "Steering flexible needles under markov motion uncertainty," in *Proc. IEEE/RSJ Int. Conf. Intell. Robot. Syst. IROS'05*, 2005, pp. 1570–1575.
- [29] R. J. Webster, J. S. Kim, N. J. Cowan, G. S. Chirikjian, and A. M. Okamura, "Nonholonomic modeling of needle steering," *Int. J. Robot. Res.*, vol. 25, no. 5–6, pp. 509–525, 2006.
- [30] W. Park, Y. Wang, and G. S. Chirikjian, "The path-of-probability algorithm for steering and feedback control of flexible needles," *Int. J. Robot. Res.*, vol. 29, no. 7, pp. 813–830, 2010.
- [31] G. Boothroyd, *Assembly Automation and Product Design*. Cambridge, U.K.: Cambridge Univ. Press, 2005, vol. 536.
- [32] G. Boothroyd and A. H. Redford, *Mechanized Assembly: Fundamentals of Parts Feeding Orientation, and Mechanized Assembly*. New York, NY, USA: McGraw-Hill, 1968.
- [33] L. S. H. De Mello and S. Lee, *Computer-Aided Mechanical Assembly Planning*. Boston, MA, USA: Kluwer, 1991, vol. 148.
- [34] A. Sanderson, "Parts entropy methods for robotic assembly system design," in *Proc. IEEE Int. Conf. Robot. Autom.*, 1984, vol. 1, pp. 600–608.
- [35] M. A. Erdmann and M. T. Mason, "An exploration of sensorless manipulation," *IEEE J. Robot. Autom.*, vol. 4, no. 4, pp. 369–379, 1988.
- [36] K. Y. Goldberg, "Orienting polygonal parts without sensors," *Algorithmica*, vol. 10, no. 2–4, pp. 201–225, 1993.
- [37] Y. Liu and R. J. Popplestone, "Symmetry groups in analysis of assembly kinematics," in *Proc. IEEE Int. Conf. Robot. Autom.*, 1991, pp. 572–577.
- [38] G. S. Chirikjian, "Parts entropy and the principal kinematic formula," in *Proc. Int. Conf. Autom. Sci. Eng.*, 2008, pp. 864–869.
- [39] M. D. Kutzer, M. Armand, D. H. Scheid, E. Lin, and G. S. Chirikjian, "Toward cooperative team-diagnosis in multi-robot systems," *Int. J. Robot. Res.*, vol. 27, no. 9, pp. 1069–1090, 2008.
- [40] K. Lee, M. Moses, and G. S. Chirikjian, "Robotic self-replication in structured environments: Physical demonstrations and complexity measures," *Int. J. Robot. Res.*, vol. 27, no. 3–4, pp. 387–401, 2008.
- [41] G. S. Chirikjian, "Parts entropy, symmetry and the difficulty of self-replication," in *ASME Dynamic Syst. Control Conf.*, 2008.
- [42] R. Coifman, Y. Shkolnisky, F. Sigworth, and A. Singer, "Reference free structure determination through eigenvectors of center of mass operators," *Appl. Comput. Harmonic Anal.*, vol. 28, no. 3, pp. 296–312, 2010.
- [43] G. Jensen, "Alignment error envelopes for single particle analysis," *J. Structural Biol.*, vol. 133, no. 2–3, pp. 143–155, 2001.
- [44] P. Baldwin and P. Penczek, "Estimating alignment errors in sets of 2-D images," *J. Structural Biol.*, vol. 150, no. 2, pp. 211–225, 2005.
- [45] G. Chirikjian, *Stochastic Models, Information Theory, and Lie Groups*. Cambridge, MA, USA: Birkhauser, 2009 and 2011, vol. I and II.
- [46] W. Park, D. Madden, D. Rockmore, and G. Chirikjian, "Deblurring of class-averaged images in single-particle electron microscopy," *Inverse Problems*, vol. 26, 2010.
- [47] J. Canny, "A computational approach to edge detection," *IEEE Trans. Pattern Analysis and Machine Intelligence*, vol. 8, no. 6, pp. 679–698, 1986.
- [48] G. Chirikjian and A. Kyatkin, *Engineering Applications of Noncommutative Harmonic Analysis*. Boca Raton, FL, USA: CRC Press, 2001.
- [49] M. Van Heel, W. Keegstra, W. Schutter, and E. van Bruggen, "Arthropod hemocyanin structures studied by image analysis," *Life Chem. Rep.*, vol. 1, pp. 69–73, 1982, Suppl.
- [50] W. Saxton and W. Baumeister, "The correlation averaging of a regularly arranged bacterial cell envelope protein," *Microscopy*, vol. 127, no. 2, pp. 127–138, 1982.



Wooram Park (S'06–M'11) received the B.S.E. and M.S.E. degrees in mechanical engineering from Seoul National University, Seoul, Korea, in 1999 and 2003, respectively, and the Ph.D. degree in mechanical engineering from Johns Hopkins University, Baltimore, MD, USA, in 2008.

He is an Assistant Professor with the Department of Mechanical Engineering, University of Texas at Dallas, Richardson, TX, USA, since 2011. His research mainly concerns medical robots, computational structural biology and design of intelligent robots. Prior to joining UT Dallas in 2011, he was a Postdoctoral Fellow in Mechanical Engineering at Johns Hopkins University.

Prof. Park is a Member of the American Society of Mechanical Engineers (ASME). He was a recipient of the Creel Family Fellowship at Johns Hopkins University in 2007.



Gregory S. Chirikjian (M'93–SM'08–F'10) received the B.A., B.S., and M.S.E. degrees from Johns Hopkins University, Baltimore, MD, USA, in 1988, and the Ph.D. degree from the California Institute of Technology, Pasadena, CA, USA, in 1992.

Since 1992, he has been on the faculty of the Department of Mechanical Engineering, Johns Hopkins University, where he has been a Full Professor since 2001. From 2004 to 2007, he served as Department Chair. He has published more than 220 works, including three books. His research interests include robotics, applications of group theory in a variety of engineering disciplines, and the mechanics of biological macromolecules.

Prof. Chirikjian is a Fellow of the American Society of Mechanical Engineers (ASME), a 1993 National Science Foundation Young Investigator, a 1994 Presidential Faculty Fellow, a 1996 recipient of the ASME Pi Tau Sigma Gold Medal.